Magnetocaloric effect of polycrystalline La$_{0.5}$Sm$_{0.2}$Sr$_{0.3}$Mn$_{1-x}$Cr$_x$O$_3$ (0 ≤ *x* ≤ 0.20) compound prepared by glycine-nitrate process

Khouloud Abdouli[1,2,*] , W. Cherif[1,2], M. A. Valent[3], M. P. F. Graça[3], L. Ktari[2], O. Messaoudi[4], S. Elgharbi[5], and W. I. Elsofany[5]

[1] *National Engineering School of Sfax, Sfax, Tunisia*

[2] *Faculty of Sciences, Sfax University, B. P. 1171, 3000 Sfax, Tunisia*

[3] *I3N - University of Aveiro, Aveiro, Portugal*

[4] *Physics Department, College of Sciences, University of Ha'il, Hail, Saudi Arabia*

[5] *Chemistry Department, College of Sciences, University of Ha'il, Hail, Saudi Arabia*

ABSTRACT

This paper reports the effect of chromium's substitution in magnetic oxides with perovskite structure La$_{0.5}$Sm$_{0.2}$Sr$_{0.3}$Mn$_{1-x}$Cr$_x$O$_3$ (*x* = 0, 0.1, 0.15 and 0.2) compounds which have been produced with the glycine-nitrate process (GNP). The four compounds have an orthorhombic crystal structure with '*Pnma*' space group. We note that they undergo a second-order paramagnetic-ferromagnetic (PM-FM) phase transition. Substitution manganese by chromium leads to a drop of the Curie temperature T$_C$ from 278 K (*x* = 0) to 205 K (*x* = 0.2). Their magnetocaloric effect has been evaluated by their magnetic entropy change $\left(-\Delta S_M^{max}\right)$ under a magnetic field change up to 5 T. All relative cooling power (RCP) suggests that these compounds are suitable candidates for magnetic refrigeration.

1 Introduction

Magnetic refrigeration (MR) based on the magnetocaloric effect (MCE) is an environment-friendly cooling technology with low energy consumption [1–3]. Its application has drawn attention not only at room temperature but even lower (e.g., gas liquefaction as helium, hydrogen, and natural gas). The MCE is an inherent property of magnetic materials, and it is the result of exposing the magnetic material to an external magnetic field or to removing it [4]. This property enables us to determine whether a magnetic material can be regarded as a good magnetic refrigerant or not. MCE can be evaluated through the calculation of magnetic entropy changes (ΔS_M) based on the isothermal magnetization data and using the Maxwell equation [5].

Address correspondence to E-mail: abdouli.khouloud2@gmail.com

$$\Delta S_M(T,H) = S_M(T,H_1) - S_M(T,H_2) = \int_{H_1}^{H_2} \left(\frac{\partial M}{\partial T}\right) dH. \tag{1}$$

For industrial applications, the efficiency of a good magnetocaloric material destined for magnetic refrigeration is evaluated in terms of a high value of magnetic entropy change ($- \Delta SM_{max}$) and a large relative cooling power (RCP) [6]. RCP is the heat transfer between the hot and cold reservoirs in the ideal refrigeration cycle, which is generally assessed using the following relation [7]:

$$RCP = \left|(-\Delta S_M^{max})\right| \times \delta T_{FWHM}, \tag{2}$$

where $\left|(-\Delta S_M^{max})\right|$ is the absolute value of the maximum magnetic entropy change and δT_{FWHM} is the temperature difference at the full width at half maximum (FWHM) of (ΔS_M) curve, with $\delta T_{FWHM} = T_2 - T_1$..

A lot of research work has been done to find the best refrigerants with potential applications at RT magnetic refrigeration, such as the study of $Gd_5(Ge_{1-x}Si_x)$ [8], $MnAs_{1-x}Sb_x$ [9], $MnFeP_{1-x}As_x$, [10], $LaFe_{13-x}Si_x$ [11], and Ni–Mn–Ga [12]. Currently, the perovskite manganite oxide with the chemical formula $Ln_{1-x}A_xMnO_3$ (Ln = trivalent rare earth, A = divalent alkaline earth) has attracted much attention due to its wide range of properties such as (MCE) [7]. The principal advantages of this type of compounds over Gd and GdSiGe alloys are low cost, high chemical stability (no oxidation), tunable T_C, low coercivity, and high electric resistance [13]. Consequently, manganites oxides have been considered as promising candidates for MR [14]. Several reports are addressing magnetic and MCE properties of a perovskite with A-site substitutions such as $Pr_{1/2}Sr_{1/2}MnO_3$ [15], $La_{0.6}Pb_{0.4}MnO_3$ [16], $Nd_{1-x}Sr_xMnO_3$ [17], $La_{1-x}Ca_xMnO_3$ [18], $Ln_{0.67}Sr_{0.33}MnO_3$ (Ln = La, Pr and Nd) [19], and Pr-doped $La_{0.67}Ca_{0.33}MnO_3$

nanoparticles [20]. Among these materials, Lanthanum manganites have attracted the attention of many researchers, thanks to the very rich phase diagram observed in $La_{1-x}Ca_xMnO_3$ and $La_{1-x}Sr_xMnO_3$ samples. Lanthanum manganites are characterized by multi-phase transitions [21–23]. In particular, $La_{1-x}Sr_xMnO_3$ perovskite manganite is an important member in the manganite family due to its significant physical properties and potential applications in high-performance magneto-resistive sensors and magnetic heads [24]. The highest Curie temperature was detected in $La_{0.7}Sr_{0.3}MnO_3$ which was about 360 K. To be used for magnetic refrigeration near room temperature, it is important to use appropriate alternative methods to reduce its T_C. In general, a partial replacement of non-magnetic ion La^{3+} with a smaller sized rare-earth magnetic ion (Sm, Nd, Gd…) leads to a decrease in the Curie temperature [25]. In other hand, research has also been carried out on the replacement of Mn site with transition elements (eg Fe, Co, Ga, Cr, etc.) [26–33]. The Cr substitution is notably interesting, since Cr^{3+} is isoelectronic with Mn^{4+} ($t_{2g}^3 e_g^0$) and is a non-Jahn–Teller ion [34]. A literature overview highlights that the ionic radius of Cr^{3+} is closely the same as that of the Mn^{3+}; therefore, it can easily substitute Mn in the manganites system. Cr substitution in the B-site of manganites affects the Mn^{3+} –O– Mn^{4+} network because it will influence the double exchange, which leads to change the physical properties of the material [35]. For an industrial achievement, a major interest is focusing on the design of simple, greener, economic, and scalable synthesis process of magnetic materials [36]. Magnetic materials have been prepared using several synthesis techniques (e.g., solid-state reaction, ball milling, sol–gel). In the recent time, auto-combustion method of glycine-nitrate precursors is considered to be the easiest, the fastest process for formation of homogeneous crystalline particles, and low external
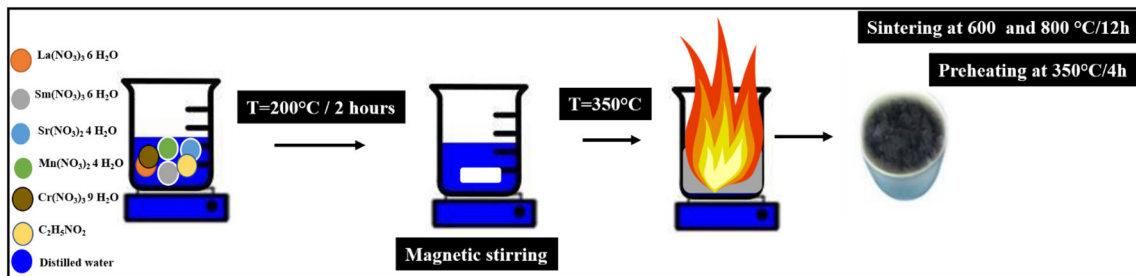

Fig. 1 Details of the auto-combustion process

energy consumption. We study in this article the effect of Cr doping on the structural, magnetic, and magnetocaloric properties of $La_{0.5}Sm_{0.2}Sr_{0.3}Mn_{1-x}Cr_xO_3$ (x = 0.00, 0.10, 0.15, and 0.20) prepared by auto-combustion method.
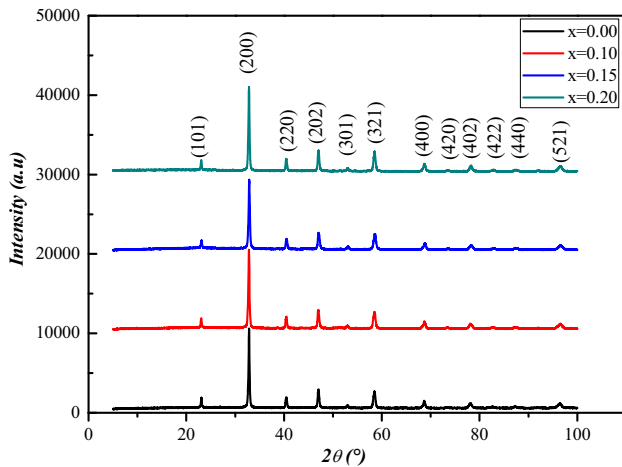
Fig. 2 X-ray diffraction pattern of $La_{0.5}Sm_{0.2}Sr_{0.3}Mn_{1-x}Cr_xO_3$ (x = 0.00, 0.10, 0.15, and 0.20)

2 Experimental procedure

2.1 Synthesis method

$La_{0.5}Sm_{0.2}Sr_{0.3}Mn_{1-x}Cr_xO_3$ (x = 0.00, 0.10, 0.15 and 0.20) powders were prepared using the auto-combustion method (See Fig. 1). Stoichiometric amount of $La(NO_3)_3$, 6 H_2O, $Sm(NO_3)_3$, 6 H_2O, $Sr(NO_3)_2$, $Mn(NO_3)_2$, 4 H_2O, $Cr(NO_3)_3$, and 9 H_2O (99.995% in purity, "Sigma Aldrich") were dissolved in distilled water. Then we add the Glycine nitrate ($C_2H_5NO_2$,- ~ 99.995% "Sigma Aldrich") to the solution which is used as a fuel. The molar ratio of glycine-nitrate was fixed on 1 in the present work. The solution was heated on a hot plate at 100 °C for 1 h with stirring. The water evaporation converted the solution to a viscous transparent gel. The auto-ignition started when the temperature reached 350 °C, the burning lasted only a few seconds, and a large amount of fine "ash" was produced. The obtained "ash" was pre-heated at 350 °C for 4 h to eliminate any carbon remainder in the powder and to form a pure-crystal structure. The calcined powder was pressed at 4 tons/cm2 to form pellets with a thickness of 1 mm and then sintered at 600 and 800° C for 12 h.

Table 1 Refinement results for the samples $La_{0.5}Sm_{0.2}Sr_{0.3}Mn_{1-x}Cr_xO_3$ (x = 0.00, 0.10, 0.15 and 0.20) determined from XRD patterns measured at room temperature

Parameters	x = 0.00	x = 0.10	x = 0.15	x = 0.20
Symmetry	Orthorhombic	Orthorhombic	Orthorhombic	Orthorhombic
Space group	Pnma	Pnma	Pnma	Pnma
a (Å)	5.5019 (2)	5.496 (5)	5.491 (4)	5.489 (9)
b (Å)	7.7321 (3)	7.718 (6)	7.713 (7)	7.717 (9)
c (Å)	5.4696 (2)	5.462 (6)	5.459 (9)	5.460 (8)
V (Å^3)	232.68 (6)	231.752 (4)	231.27 (6)	231.376 (8)
d_{Mn-O_1}(Å)	1.939 (5)	1.950 (4)	1.949 (4)	1.955 (4)
d_{Mn-O_2}(Å)	2.11 (3)	1.99 (3)	1.86 (6)	1.87 (3)
d_{Mn-O_2}(Å)	1.82 (3)	1.92 (3)	2.02 (6)	2.03 (3)
d_{Mn-O}(Å)	1.958 (5)	1.955 (4)	1.947 (1)	1.953 (8)
θ_{Mn-O_1-Mn}(°)	170.6 (2)	163.36 (17)	163.37 (16)	161.44 (15)
θ_{Mn-O_2-Mn}(°)	162.4 (12)	165.2 (14)	170. (3)	166.4 (12)
$\theta_{Mn-O-Mn}$(°)	166.51 (6)	164.28 (7)	166.835 (8)	163.926 (7)
R_p (%)	3.32	3.19	3.39	3.74
R_{wp} (%)	4.21	4.04	4.25	4.79
R_{exp} (%)	3.67	3.61	3.73	4.16
Brag R-Factor (%)	1.83	1.78	1.59	1.57
RF-Factor (%)	3.86	4.34	3.33	3.19
χ^2 (%)	1.31	1.25	1.30	1.33

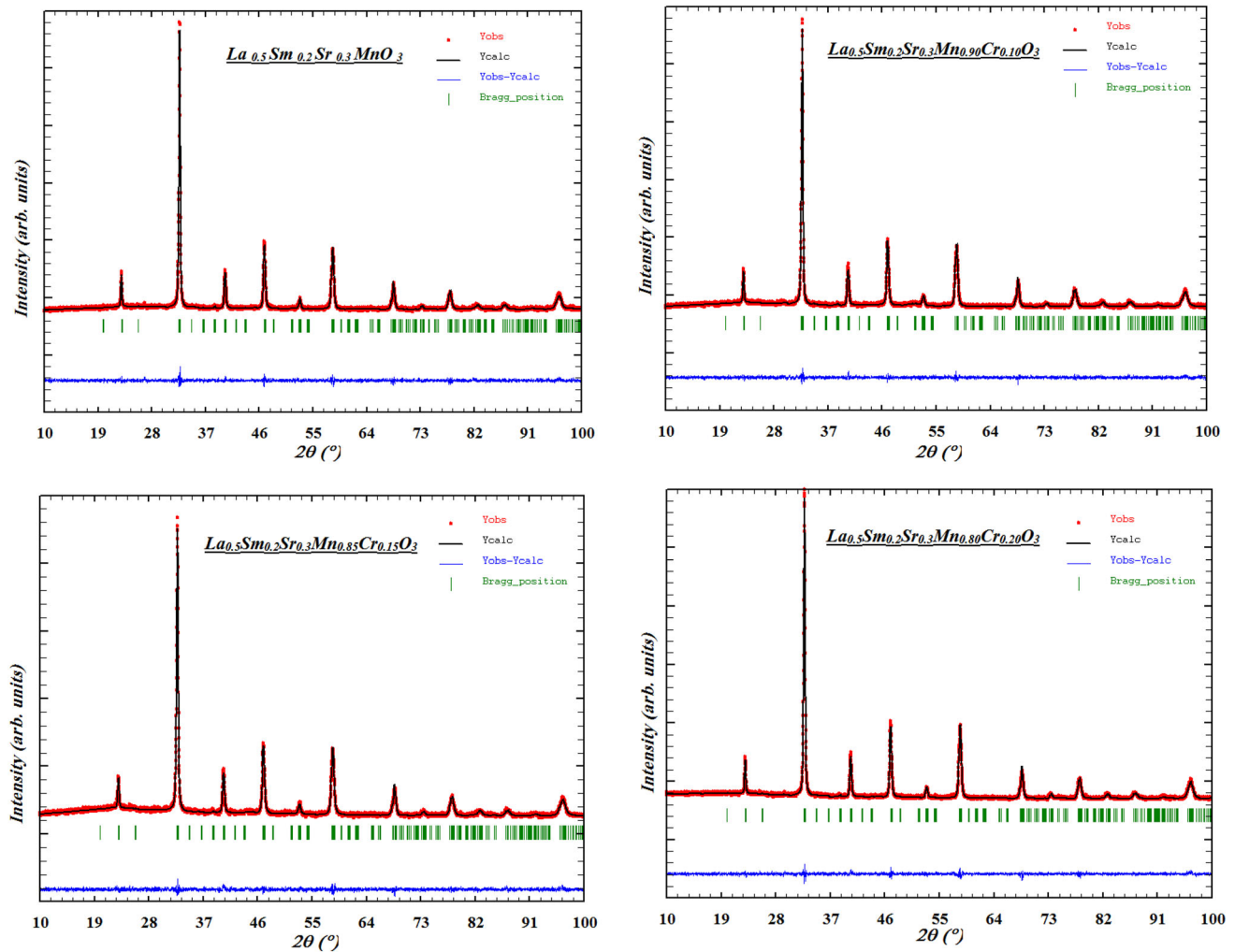**Fig. 3** Observed and calculated X-ray diffraction data and Rietveld refinement for $La_{0.5}Sm_{0.2}Sr_{0.3}Mn_{1-x}Cr_xO_3$ ($x = 0.00$, 0.10, 0.15, and 0.20). Vertical bars are the Bragg reflections for the space group Pnma. The difference pattern between the observed data and fits are shown at the bottom

2.2 Characterization techniques

2.2.1 X-ray powder diffraction

The phase purity, crystal structure, and lattice parameters have been examined using the X-ray powder diffraction (XRD) at room temperature. XRD patterns were collected by a Phillips powder diffractometer PW 1710 using Cu Kα radiation ($\lambda = 1.5405$Å).

The diffraction data were analyzed by the Rietveld method using the FULLPROF software [37].

2.2.2 FTIR—Fourier Transformation Infrared—spectroscopy analysis

To identify the functional group of the prepared samples, we use the FTIR analysis. Nicolet Impact 400 Spectrophotometer was used to record FTIR spectra in the wavenumber range of 400–4000 cm^{-1} at RT.

2.2.3 Vibrating sample magnetometer (VSM)

A vibrating sample magnetometer (VSM) was used to record the magnetic measurements value with a constant applied magnetic field of 0.1 T under the conditions of zero-field cooled (ZFC) and field cooled (FC) in the temperature range of 5–300 K.
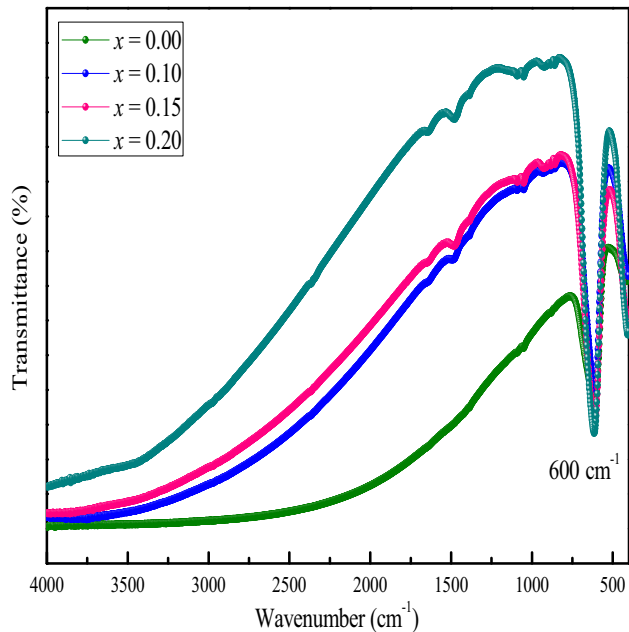
Fig. 4 FTIR spectra of $La_{0.5}Sm_{0.2}Sr_{0.3}$ $Mn_{1-x}Cr_xO_3$ ($x = 0.00$, 0.10, 0.15 and 0.20) compounds

Table 2 Magnetic parameters for $La_{0.5}Sm_{0.2}Sr_{0.3}Mn_{1-x}Cr_xO_3$ ($x = 0.00$, 0.10, 0.15, and 0.20) compounds

x	T_C (K)	θ_p (K)	C (μ_B.K/T)	$\mu_{eff}^{exp}(\mu_B)$	$\mu_{eff}^{th}(\mu_B)$
0.00	278	283.659 (6)	8.64	7.724 (4)	4.630
0.10	264	280.045 (1)	7.10	6.347 (6)	4.532
0.15	245	262.768 (9)	5.75	5.140 (6)	4.482
0.20	205	255.034 (4)	4.77	4.264 (5)	4.431

Isothermal measurements M (H) were carried out by varying H up to 5 T at different Ts.

3 Results and discussions

3.1 Structural analysis

The Rietveld refinement of X-ray diffraction patterns confirms that all compounds are single phase with orthorhombic structural, Pnma space group (See Figs. 2 and 3). Table 1 shows information about the relevant structural parameters obtained by Rietveld refinements. A reduction of the unit cell volume and the lattice parameters is expected upon substitution manganese by chromium because the radius of Cr^{3+}

(0.615 Å) is a little smaller than that of Mn^{3+} (0.645 Å) [38]. The bond lengths dMn–O and the bond angle Mn–O–Mn change slightly with increasing Cr^{3+} content.

3.2 Fourier transformation infrared spectroscopy

In order to detect the absorption bands in the prepared samples, Fourier transformation infrared spectroscopy analysis was performed at room temperature in the wave number range of 400–4000 cm^{-1}. The FTIR spectrums are presented in Fig. 4. The main absorption bands are observed at around 600 cm^{-1}. These absorption bands can be attributed to Mn–O and O–Mn–O bond vibrations of the octahedral MnO_6 in our perovskite structure samples [39, 40].

3.3 Magnetic properties

Figure 5 displays the temperature dependence of magnetization (M) of $La_{0.5}Sm_{0.2}Sr_{0.3}Mn_{1-x}Cr_xO_3$ samples in the (ZFC) and (FC) processes measured with the application of a magnetic field of 0.1 T. It can be seen that the FC curves exhibit a single (PM-FM) behavior transition with decreasing T. At an irreversibility temperature (T_{irr}), a bifurcation between the FC and ZFC curves and a drop in ZFC magnetization (λ shape) are observed which can be associated to super para-magnetism or spin glass behavior [41–43]. Similar behavior was observed in $La_{0.5}Sm_{0.2}Sr_{0.3}Mn_{1-x}Fe_xO_3$ compounds reported by Kh. Abdouli et al. [29].

Curie temperature (T_C) is the temperature where the (PM-FM) transition occurs and is estimated from the peak of dM/dT (T) curves (inset of Fig. 5). The T_C values for the samples ($x = 0.00$, 0.10, 0.15, and 0.20) are given in Table 2. Substitution of Cr at the Mn site causes a gradually reduction in Curie temperature from 278 to 205 K for $x = 0.00$ and $x = 0.20$.

The decrease of T_C is related to the decrease of Mn ion rate and the increase of Cr ion concentration. Cr^{3+} ions can basically replace Mn^{3+} ions. Indeed, $r_{<Cr^{3+}>}$ = (0.615 Å) is smaller than $r_{<Mn^{3+}>}$ = (0.645 Å) and bigger than $r_{<Mn^{4+}>}$ = (0.53 Å). Furthermore, Cr^{3+} ion has an electronic configuration similar to Mn^{4+} ion ($t_{2g}^3 e_g^0$) which lead to the appearance of an antiferromagnetic super exchange interaction between Cr^{3+} and Mn^{4+} [44]. The increase of the content of
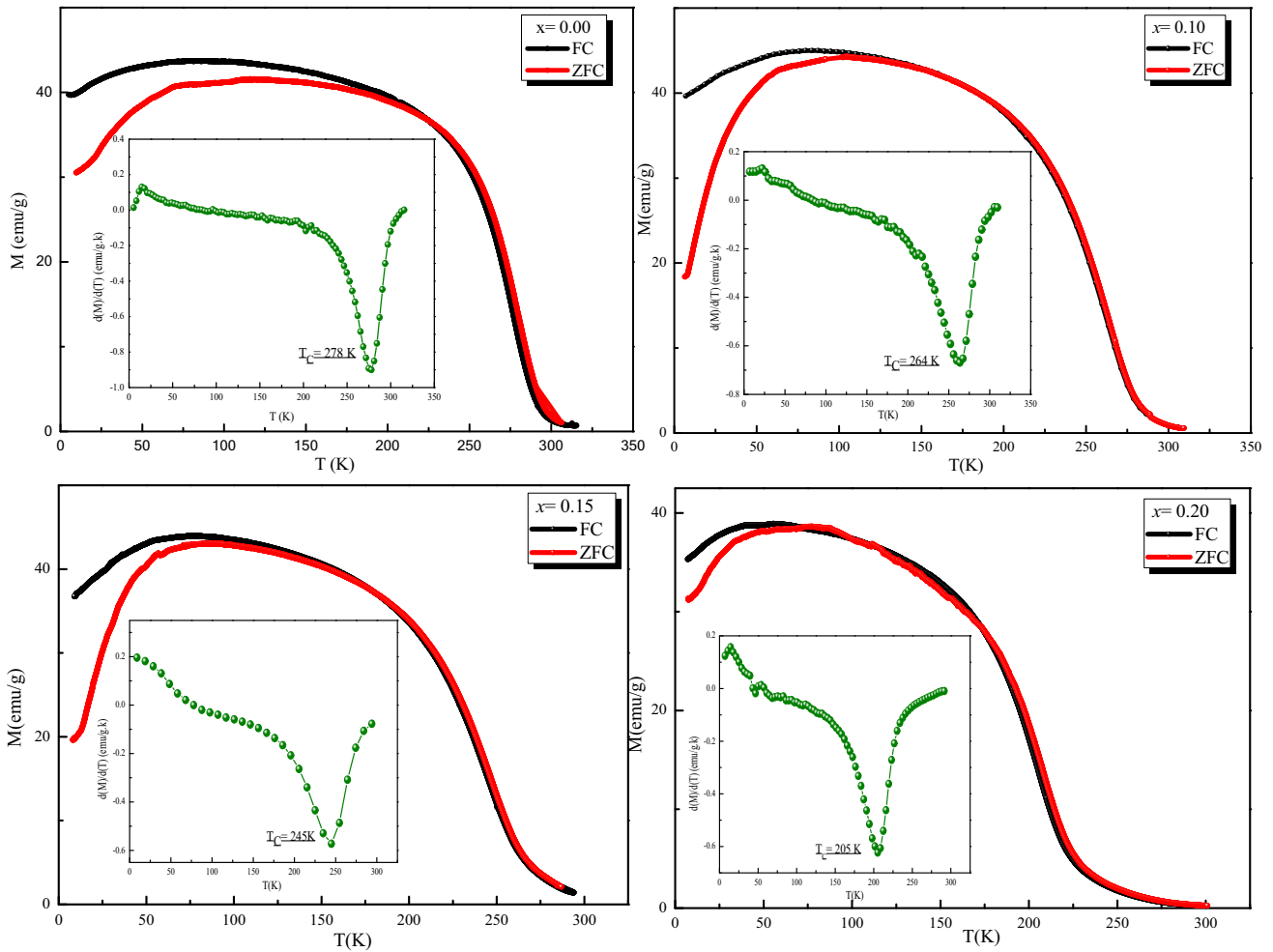
Fig. 5 Variation of the magnetization (M) vs. temperature (T) of La$_{0.5}$Sm$_{0.2}$Sr$_{0.3}$ Mn$_{1-x}$Cr$_x$O$_3$ (x = 0.00, 0.10, 0.15 and 0.20) compounds measured at an applied magnetic field of 0.1 T. Inset: The variation of dM/dT as a function of temperature (T)

Cr^{3+} ion significantly decreases Mn^{3+}/ Mn^{4+} ratio which means that the double-exchange interactions between Mn^{3+} and Mn^{4+} ions was partially destroyed, while the antiferromagnetic interactions between Cr^{3+} and Mn^{4+} are enhanced. Also, the antiferromagnetic coupling between Mn^{4+}-Mn^{4+} and Cr^{3+}-Cr^{3+} should be considered. To sum up, ferromagnetic double-exchange interactions are weakened when Mn is substituted by Cr, while the antiferromagnetic interactions are reinforced.

Furthermore, in order to know the magnetic behavior in the paramagnetic range, we studied the temperature dependence of the inverse magnetic susceptibility (χ), which is plotted from the M (T) data and shown in (Fig. 6). The fit of ($1/\chi$) as a function of temperature reveals that at high temperature, the four samples follow the Curie–Weiss behavior:

$$\chi = \frac{C}{T - \theta_p} \tag{3}$$

where χ is the susceptibility, θ_P is the Curie–Weiss temperature and C is the Curie constant.

It can be noted that θ_P values are slightly higher than that of T_C, their positive values indicate that there is a ferromagnetic exchange interaction between the nearest neighbors. In general, this difference between θ_P and T_C depends on the material and is related with the existence of short range ordered slightly above T_C, which is associated to the existence of a magnetic inhomogeneity.

According to the determined Curie constant (C), the known relation

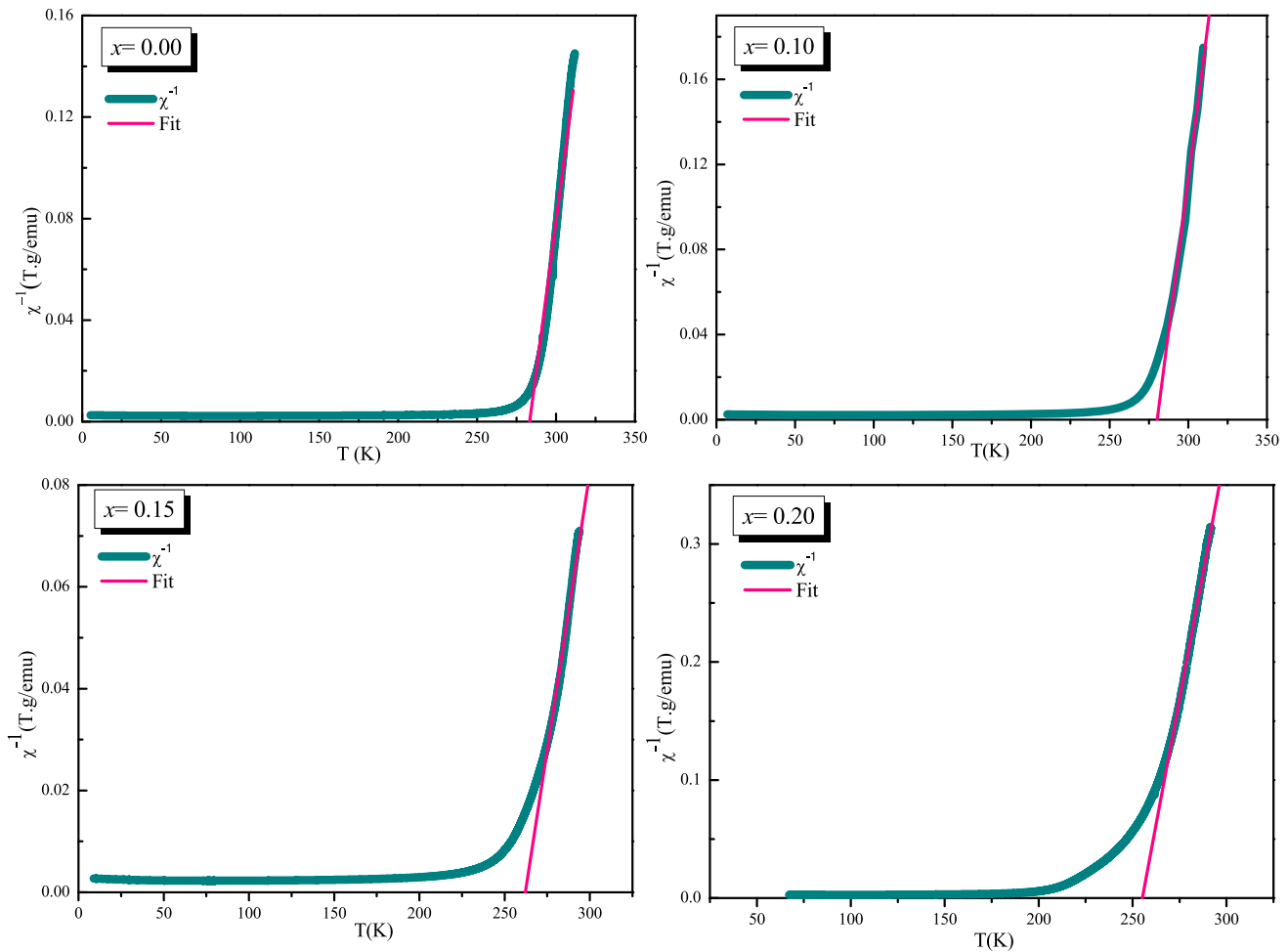$$(\mu_{eff}^{exp})^2 = \frac{3K_B M_m}{N_A \mu_B^2} C \tag{4}$$

Fig. 6 Variation of the inverse magnetic susceptibility (χ^{-1}) as function of temperature, and the red lines are the fits according to the Curiee-Weiss law

is used to determine the experimental effective paramagnetic moments (μ_{eff}^{exp}),. where N_A is the Avogadro's number (6.023×10^{23} atoms mol^{-1}), μ_B is the Bohr magneton (9.274×10^{-21}), M_m is the molecular weight, and K_B is the Boltzmann constant (1.38016×10^{-16} erg K^{-1}).

According to $La_{0.5}Sm_{0.2}Sr_{0.3}Mn_{1-x}Cr_xO_3$ composition, the theoretical effective paramagnetic moment is determined via the following relation:

θ_P, μ_{eff}^{exp}, and μ_{eff}^{th} values are registered in Table 2.

The dissimilarity between μ_{eff}^{exp} and μ_{eff}^{th} values may be related to the existence of the ferromagnetic polarons in the paramagnetic state [45].

3.3.1 Isothermal magnetization studies

To understand the magnetism and to approve the ferromagnetic comportment of the samples at low

$$\mu_{eff}^{th} = \sqrt{0.2[\mu_{eff}^{th}(Sm^{3+})]^2 + (0.7 - x)[\mu_{eff}^{th}(Mn^{3+})]^2 + x[\mu_{eff}^{th}(Cr^{3+})]^2 + 0.3[\mu_{eff}^{th}(Mn^{4+})]^2},$$ (5)

where $\mu_{eff} = 0.85\mu_B$ for Sm^{3+}, $\mu_{eff} = 4.9\mu_B$ for Mn^{3+}, $\mu_{eff} = 3.87\mu_B$ for Mn^{4+}, and $\mu_{eff} = 3.87\mu_B$ for Cr^{3+}.

temperatures, we report in Fig. 7 the relationship between the magnetization (M) and the applied
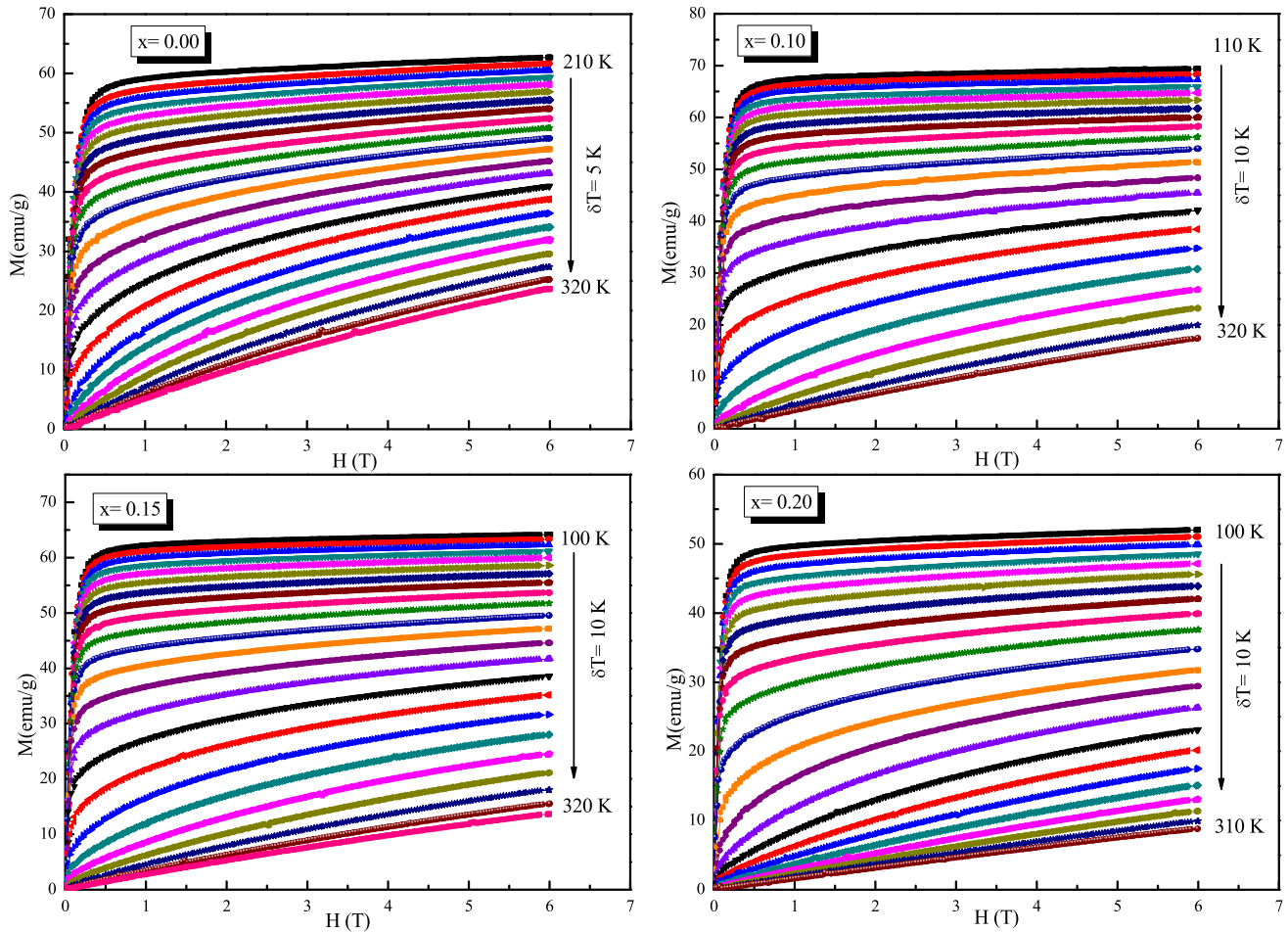
Fig. 7 Isothermal magnetization for $La_{0.5}Sm_{0.2}Sr_{0.3}Mn_{1-x}Cr_xO_3$ ($x = 0.00$, 0.10, 0.15, and 0.20) samples measured at different temperatures around T_C

magnetic field (H) at several temperatures near to T_C (up to 5 T). It can be observed that M (H) curves, near the FM-PM transition, gradually increase with increasing H values. Below T_C, a typical behavior of ferromagnetic material is detected, after applying a magnetic field up to 1 T, the magnetization rises sharply and then reaches saturation. Above T_C, the magnetization M increases more steadily, and the M (H) curves gradually become linear, which is common in paramagnetic materials. It can be clearly seen from Fig. 7 that an increase in temperature will cause a slight decrease in magnetization. This reduction is mainly due to the magnetic moment disorder caused by thermal stirring.

3.3.2 Arrott curves

In order to further understand the nature of the FM-PM phase transition, we derive the Arrott plots (H/M vs. M^2) from M(H) plots [46] for the four samples as shown in Fig. 8. Arrott plots are usually used to determine the sequence of magnetic phase transitions. Indeed, as reported by the criterion suggested by Banerjee [47], the negative slope corresponds to the first-order magnetic transition, and the positive slope corresponds to the second-order magnetic transition. It can be clearly seen from Fig. 8 that the Arrott plots show a positive slope, confirming the second-order nature of the phase transition from FM to PM. This approves the results already seen in the discussion section of M (T).
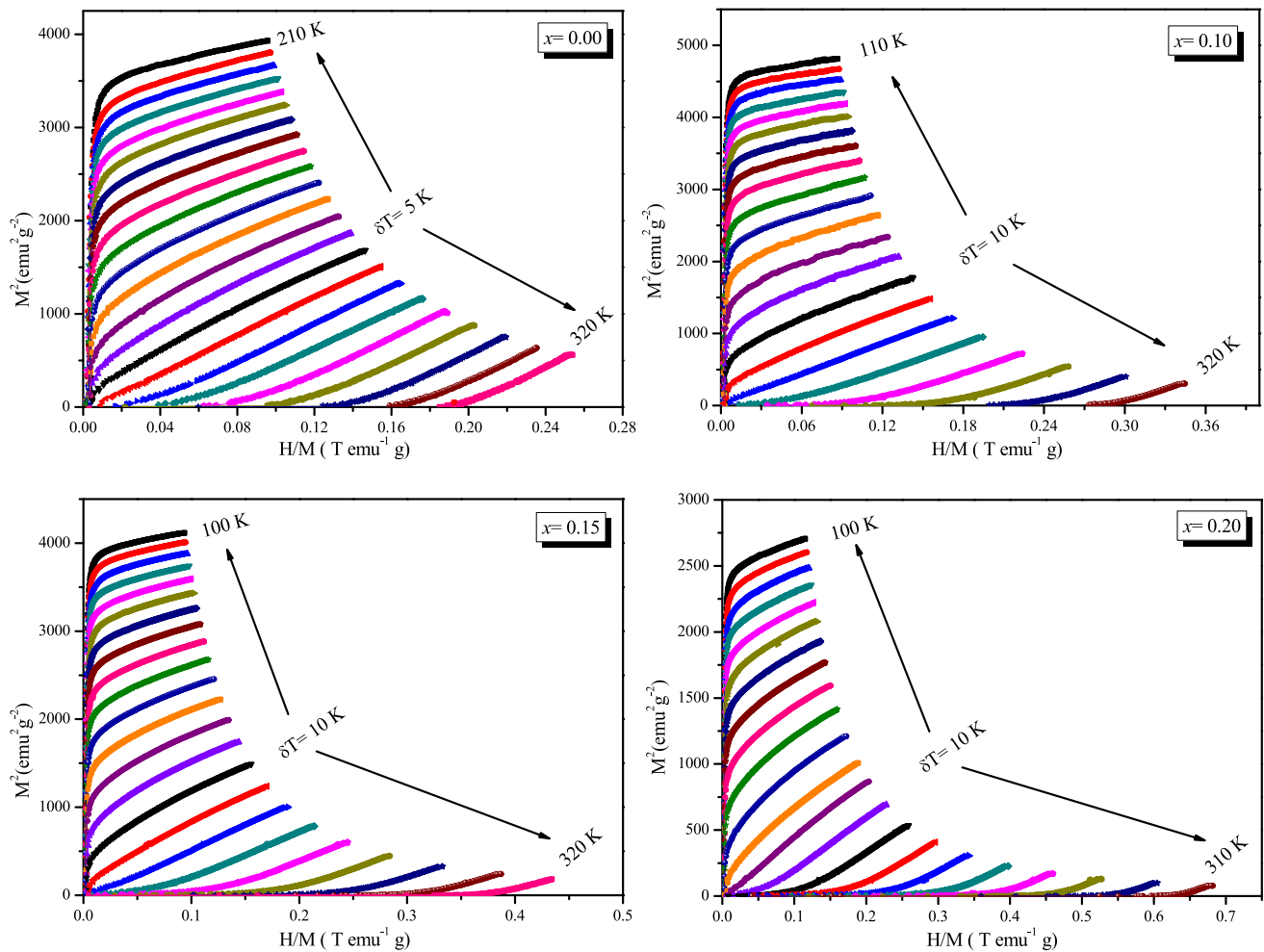
Fig. 8 Arrott plots (M_2 vs. $\mu_0 H/M$) of $La_{0.5}Sm_{0.2}Sr_{0.3}Mn_{1-x}Cr_xO_3$ (x = 0.00, 0.10, 0.15 and 0.20) samples around T_C

3.4 Magnetocaloric effect

Figure 9 shows the temperature dependence of the magnetic entropy changes ($-\Delta S_M$) for our four samples when the magnetic field change is at most 5 T. It is found that ($-\Delta S_M$) rises with the rising of temperature, thus, reaching the maximum value at T_C. The characteristics of the magnetic transition can be concluded from the sign of ($-\Delta SM$) (T, H). For materials presenting a FM transition, we found positive values of ($-\Delta S_M$) (T, H) due to the formation of a magnetically ordered configuration when an external magnetic field is applied [48]. As the magnetic field increases, the magnetization and spin alignment increase, followed by the increase in the maximum magnetic entropy change value ($-\Delta S_M^{max}$) of all compounds. However, due to the secondary nature of the ferromagnetic transition in these compounds, the peak position is hardly affected. It is found that ($-\Delta S_M^{max}$) is influenced by the Cr doping. In fact, under H = 5 T ($-\Delta S_M^{max}$) is 3.06 J kg^{-1} K^{-1} at 277 K, 2.44 J kg^{-1} K^{-1} at 269 K, 2.30 J kg^{-1} K^{-1} at 254 K, and 1.92 J kg^{-1} K^{-1} at 204 K for x = 0.00, 0.10, 0.15, and 0.20 (Fig. 9).

The values of our entropy change decrease with Cr^{3+} substitution increases. We can explain this result by the decreasing number of hopping electrons and the reduction of DE interactions of Mn^{3+}-O-Mn^{4+}. As previously mentioned, such as Cr^{3+} replaces Mn3 + , the replacement of Mn site by trivalent ions reduces Mn^{3+}/Mn^{4+} rate and the lattice will be affected due to the presence of Cr^{3+} in Mn–O–Mn chains. The chromium substitution reduces the DE interaction and the magnitude of the ($-\Delta S_M^{max}$).
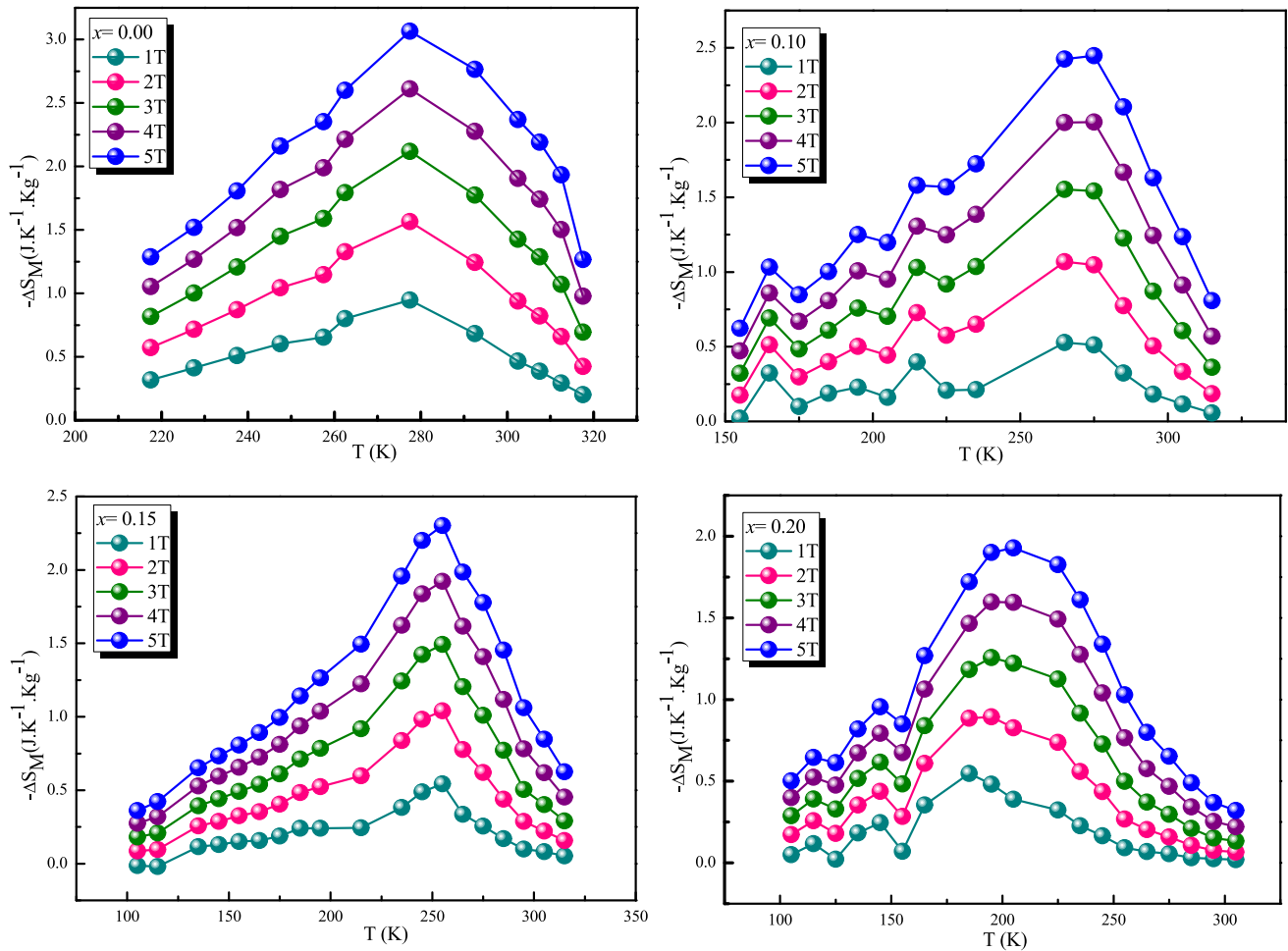
Fig. 9 Magnetic entropy change ($-\Delta S_M$) as a function of temperature in various magnetic fields between 1 and 5 T of the compounds $La_{0.5}Sm_{0.2}Sr_{0.3}Mn_{1-x}Cr_xO_3$ (x = 0.00, 0.10, 0.15, and 0.20)

We list the $\left(-\Delta S_M^{max}\right)$ and RCP values of all samples in Table 3 and compare them with other results reported in the literature. It is noticed that RCP values increase with rising the applied magnetic field. This can be the result of spin coupling, which is weaker when a high magnetic field is applied.

At 5 T, RCP values are 268 J Kg^{-1}, 243 J Kg^{-1}, 244 J Kg^{-1}, and 190 J Kg^{-1} for x = 0.00, 0.10, 0.15, and 0.20, respectively. The RCP values of our compounds are about 50% of the RCP value of pure Gd, indicating that our compounds may be candidate materials for magnetic refrigeration.

4 Conclusion

In this work, the effect of partial replacement of Manganese by Chromium on structure, magnetic, and magnetocaloric properties of $La_{0.5}Sm_{0.2}Sr_{0.3}Mn_{1-x}Cr_xO_3$ (x = 0.00, 0.10, 0.15, and 0.20) compounds is studied. The four prepared compounds are crystallized at room temperature in the orthorhombic structure with Pnma space group. Magnetization measurement results show a second-order paramagnetic–ferromagnetic transition. T_C value decreases from 278 K (x = 0.00) to 205 K (x = 0.20). The

Table 3 Summary of the maximum magnetic entropy change (− ΔSM$_{max}$), δT_{FWHM} and RCP values, under a magnetic field (H) for some magnetocaloric materials

x	H (T)	$(-\Delta S_M^{max})$ (J/kg K)	δT_{FWHM}(K)	RCP (JKg^{-1})	References
La$_{0.5}$Sm$_{0.2}$Sr$_{0.3}$MnO$_3$	1	0.95 (5)	67.99 (3)	64.97 (4)	Present work
	2	1.57 (3)	76.35 (5)	120.15 (2)	Present work
	3	2.11 (7)	82.53 (7)	174.77 (2)	Present work
	4	2.62 (4)	84.71 (8)	222.32 (5)	Present work
	5	3.06 (9)	87.26 (4)	267.83 (9)	Present work
La$_{0.5}$Sm$_{0.2}$Sr$_{0.3}$Mn$_{0.90}$Cr$_{0.10}$O$_3$	1	0.51 (5)	51.01 (6)	26.30 (8)	Present work
	2	1.05 (5)	86.08 (9)	90.86 (6)	Present work
	3	1.54 (5)	91.40 (3)	141.26 (3)	Present work
	4	2.00 (0)	95.12 (3)	190.25 (5)	Present work
	5	2.44 (1)	99.90 (6)	243.87 (0)	Present work
La$_{0.5}$Sm$_{0.2}$Sr$_{0.3}$Mn$_{0.85}$Cr$_{0.15}$O$_3$	1	0.53 (5)	56.91 (7)	30.46 (1)	Present work
	2	1.04 (2)	83.83 (7)	87.43 (3)	Present work
	3	1.49 (4)	96.14 (4)	143.65 (8)	Present work
	4	1.92 (3)	101.52 (8)	195.32 (9)	Present work
	5	2.30 (4)	106.14 (2)	244.59 (3)	Present work
La$_{0.5}$Sm$_{0.2}$Sr$_{0.3}$Mn$_{0.80}$Cr$_{0.20}$O$_3$	1	0.54 (1)	65.72 (7)	35.55 (8)	Present work
	2	0.89 (6)	83.90 (7)	75.18 (0)	Present work
	3	1.25 (8)	90.20 (1)	113.47 (1)	Present work
	4	1.59 (4)	95.09 (5)	151.58 (1)	Present work
	5	1.92 (3)	99.29 (1)	190.93 (4)	Present work
Gd	5	10.2	–	410	[1]
Sm$_{0.58}$Sr$_{0.42}$MnO$_3$	5	9.3	–	302	[49]
Sm$_{0.15}$Pr$_{0.4}$Sr$_{0.45}$MnO$_3$	5	3.98	–	240	[50]
La$_{0.67}$Sr$_{0.33}$MnO$_3$	5	1.69	–	211	[51]
La$_{0.7}$Sr$_{0.3}$MnO$_3$	5	2.31	–	69	[52]
La$_{0.7}$Sr$_{0.3}$Mn$_{0.93}$Fe$_{0.07}$O$_3$	5	4	–	225	[53]
La$_{0.7}$Sr$_{0.3}$Mn$_{0.9}$Al$_{0.1}$O$_3$	5	2.6	–	109	[54]
La$_{0.7}$Ca$_{0.3}$MnO$_3$	5	6.42	–	–	[55]
La$_{0.75}$Ca$_{0.25}$MnO$_3$	5	6.25	–	198	[56]
La$_{0.75}$Ca$_{0.2}$Na$_{0.05}$MnO$_3$	5	6.35	–	270.5	[56]
La$_{0.75}$Ca$_{0.15}$Na$_{0.10}$MnO$_3$	5	6.44	–	317.7	[56]
La$_{0.7}$Ca$_{0.3}$MnO$_3$	1.8	7.43	–	93.29	[57]
La$_{0.7}$Ca$_{0.2}$Sr$_{0.1}$MnO$_3$	1.8	6.29	–	65.51	[57]
La$_{0.7}$Te$_{0.3}$MnO$_3$	5	7.16	–	266.94	[58]
La$_{0.7}$ (Te$_{0.8}$Pb$_{0.2}$)$_{0.3}$MnO$_3$	5	4.52	–	192.10	[58]

magnetocaloric properties of these compounds are checked based on the relationship between the isothermal magnetization and the magnetic field. These data are measured at different temperatures around T_C. The maximum magnetic entropy change $(-\Delta S_M^{max})$ of our samples decreases with the increase of added chromium's rate. The RCP values are also studied and are sufficiently high to make the present compounds' good candidates for near-room magnetic refrigeration.

References

1. D. Mazumdar, K. Das, I. Das, Effect of short range ferromagnetic interaction on magnetocaloric properties of polycrystalline Eu$_{0.55}$ Sr$_{0.45}$MnO$_3$ compound. J. Magn. Magn. Mater. **502**, 166507 (2020)

2. M.S. Anwar, F. Ahmed, S.R. Lee, R. Danish, B.H. Koo, Study of a-site disorder dependent structural, magnetic, and magnetocaloric properties in $La_{0.7}$-$xSmxCa_{0.3}MnO_3$ manganites. Jpn. J. Appl. Phys. **52**(10), 1–5 (2013)

3. A. Loudaini, M. Aggour, L. Bahmad, O. Mounkachi, Magnetic properties, magnetocaloric effect and cooling performance of Al Fe2 B2 compound: Ab initio, Monte Carlo and numerical modeling study. Mater. Sci. Eng. **264**, 114935 (2021)

4. Y. Zhang, Review of the structural, magnetic and magnetocaloric properties in ternary rare earth RE_2T_2X type intermetallic compounds. J. Alloy. Compd. **787**, 1173–1186 (2019)

5. V.K. Pecharsky, K.A. Gschneidner, Magnetocaloric effect and magnetic refrigeration. J. Magn. Magn. Mater. **200**, 44–56 (1999)

6. D.T. Morelli, A.M. Mance, J.V. Mantese, A.L. Micheli, Magnetocaloric properties of doped lanthanum manganite films. J. Appl. Phys. **79**(1), 373–375 (1996)

7. V.M. Andrade, R.C. Vivas, S.S. Pedro, J.C.G. Tedesco, A.L. Rossi, A.A. Coelho, M.S. Reis, Acta Mater **102**, 49–55 (2016)

8. V.K. Pecharsky, K.A. Gschneidner, Phys. Rev. Lett. **78**, 4494 (1997)

9. H. Wada, Y. Tanabe, Appl. Phys. Lett. **79**, 3302 (2001)

10. E. Brück, M. Ilyn, A.M. Tishin, O. Tegus, Magnetocaloric effects in $MnFeP_{1-x}As_x$-based compounds. J. Magn. Magn. Mater. **290–291**, 8–13 (2005)

11. B.G. Shen, J.R. Sun, F.X. Hu, H.W. Zhang, Z.H. Cheng, Adv. Mater. **21**, 4545 (2009)

12. J. Marcos, A. Planes, L. Mañosa, F. Casanova, X. Batlle, A. Labarta, Phys. Rev. B **66**, 224413 (2002)

13. A. Biswas, T. Samanta, S. Banerjee, I. Das, Observation of large low field magnetoresistance and large magnetocaloric effects in polycrystalline $Pr_{0.65}$ $(Ca_{0.7} Sr_{0.3})_{0.35}$ MnO_3. Appl. Phys. Lett. **92**(1), 2006–2009 (2008)

14. R. M'Nassri, W. Cheikhrouhou-Koubaa, M. Koubaa, N. Boudjada, A. Cheikhrouhou, Magnetic and magnetocaloric properties of $Pr_{0.6}$-$xEu xSr_{0.4}MnO_3$ manganese oxides. Solid State Commun. **151**, 1579–1582 (2011)

15. A. Biswas, I. Das, C. Majumdar, J Appl Phys **98**, 124310 (2005)

16. T. Zhang, G. Li, T. Qian, J.F. Qu, X.Q. Xiang, X.G. Li, Effect of particle size on the structure and magnetic properties of $La_{0.6}Pb_{0.4}MnO3$ nanoparticles. J ppl Phys **100**, 09432 (2006)

17. I.Z. Al-Yahmadi, A. Gismelssed, I.A. Abdel-Latif, F. Al Ma'Mari, A. Al-Rawas, S. Al-Harthy, I.A. Al-Omari, A. Yousf, H. Widatallah, M. ElZain, T.Z. Myint, Giant magnetocaloric effect and magnetic properties of nanocomposites of manganite Nd1-xSrxMnO3 ($0.0 \leq x \leq 0.8$) synthesized using modified Sol-Gel method. J. Alloys Compd. **857**, 157566 (2020)

18. A. Martinelli, M. Ferretti, C. Castellano, M.R. Cimberle, R. Masini, D. Peddis, C. Ritter, Structural, microstructural and magnetic properties of $(La_{1-x}Ca_x)MnO_3$ nanoparticles. J. Phys. Condens Matter. **25**, 17600 (2013)

19. G.F. Wang, L.R. Li, Z.R. Zhao, X.Q. Yu, X.F. Zhang, Structural and magnetocaloric effect of $Ln_{0.67}Sr_{0.33}MnO_3$ (Ln=La, Pr and Nd) nanoparticles. Ceram. Int. **40**, 16449–16454 (2014)

20. W. Xia, H. Wu, P. Xue, X. Zhu, Microstructural, magnetic, and optical properties of Pr-doped perovskite manganite $La_{0.67}Ca_{0.33}MnO3$ nanoparticles synthesized via sol-gel process. Nanoscale Res. Lett. **13**, 135 (2018)

21. Y. Tokura, features of colossal magnetoresistive manganites. Rep. Prog. Phys. **69**, 797–851 (2006)

22. A.J. Millis, Lattice effects in magnetoresistive manganese perovskites. Nature **392**, 147–150 (1998)

23. A. Urushibara, Y. Moritomo, T. Arima, A. Asamitsu, G. Kido, Y. Tokura, Insulator-metal transition and giant magnetoresistance in $La_{1-x}Sr_xMnO_3$. Phys. Rev. B. **51**, 14103–14109 (1995)

24. P.R. Broussard, S.B. Qadri, V.M. Browning, V.C. Cestone, Characterization of transport and magnetic properties in thin film $La_{0.67}(CaxSr1-x)_{0.33}MnO3$ mixtures. J. Appl. Phys. **85**, 6563–6566 (1999)

25. Q. Song, G. Wang, G. Yan, Q. Mao, W. Wang, Z. Peng, Influence of the substitution of Sm, Gd, and Dy for La in La07Sr03MnO3 on its magnetic and electric properties and strengthening effect on room-temperature CMR. J. Rare Earths **26**, 821–826 (2008)

26. A. Mleiki, S. Othmani, W. Cheikhrouhou-Koubaa, A. Cheikhrouhou, E.K. Hlil, Enhanced relative cooling power in Ga-doped $La_{0.7}(Sr, Ca)_{0.3}MnO3$ with ferromagnetic-like canted state. RSC Adv. **59**, 54299–54309 (2016)

27. P. Tiwari, D. Gangwar, C. Rath, Studies on structural, magnetic and electrochemical properties of GdMn1-xFexO3 (x= 0, 0.1 and 0.2) Perovskite compound. New J. Chem. (2021). https://doi.org/10.1039/D1NJ02026A

28. A.G. Gamzatov, A.B. Batdalov, A.M. Aliev, Z. Khurshilova, M. Ellouze, F. Ben Jemma, Specific heat, thermal diffusion, thermal conductivity and magnetocaloric effect in $Pr_{0.6}Sr_{0.4}$-Mn1−xFexO3 manganites. JMMM **443**(1), 352–357 (2017)

29. Kh. Abdouli, W. Cherif, H. Omrani, M. Mansouri, M.A. Valent, M.P.F. Graça, L. Ktari, J. Magn. Magn. Mater. **475**, 635–642 (2018)

30. A. Gómez, E. Chavarriaga, J.L. Izquierdo, J. Prado-Gonjal, F. Mompean, N. Rojas, O. Morán, Assessment of the relationship between magnetotransport and magnetocaloric properties

in nano-sized La07Ca03Mn1−xNixO3 manganites. JMMM **469**, 558–569 (2019)

31. A. Guedri, S. Mnefgui, S. Hcini, E.K. Hlil, A. Dhahri, B-site substitution impact on structural and magnetocaloric behavior of $La_{0.55}Pr_{0.1}Sr_{0.35}Mn1-xTixO3$ manganites. J. Solid State Chem. **297**, 122046 (2021)

32. R. M'assri, A. Selmi, N. ChnibaBoudjada, A. Cheikhrouhou, Field dependence of magnetocaloric properties of 20% Cr-doped $Pr_{0.7}Ca_{0.3}MnO3$ perovskite. J. Thermal Anal. Calorimetry **129**, 53–64 (2017)

33. M. Abassi, J. Dhahri, E.K. Hlil, Theoretical work on magnetocaloric effect in $La_{0.67}Ba_{0.23}Ca_{0.10}Mn_{0.90}Cr_{0.10}O3$ manganite. J. Supercond. Nov. Magn. **28**, 2455–2459 (2015)

34. V. Markovich, I. Fita, R. Puzniak, C. Martin, A. Wisniewski, C. Yaicle et al., Instability of magnetism in $Pr_{0.5}Ca_{0.5}Mn1-xCrxO3$ (x = $_{0.015}$,003): competition between pressure and thermal cycling effects. Phys. Rev. B **73**(22), 224423 (2006)

35. V.S. Kumar, R. Mahendiran, Effect of impurity doping at the Mn-site on magnetocaloric effect in $Pr_{0.6}Ca_{0.4}Mn_{0.96}B_{0.04}O3$ (B = Al, Fe, Cr, Ni Co, and Ru). J Appl Phys. **109**(2), 1023903 (2011)

36. R.S. Yadav et al., Structural, magnetic, dielectric, and electrical properties of $NiFe_2O_4$ spinel ferrite nanoparticles prepared by honey-mediated sol-gel combustion. J. Phys. Chem. Solids **107**(February), 150–161 (2017)

37. H.M. Rietveld, A profile refinement method for nuclear and magnetic structures. J. Appl. Crystallogr. **2**(2), 65–71 (1969)

38. R.D. Shannon, Revised effective ionic radii and systematic studies of interatomic distances in halides and chalcogenides. Acta Crystallogr. Sect. A **32**(5), 751–767 (1976)

39. A. Arulraj, C.N.R. Rao, An infrared spectroscopic study of the insulator-metal transition and charge-ordering in rare earth manganates, Ln1-xAxMnO3 (Ln = rare earth, A = Ca, Sr, Pb). J. Solid State Chem. **145**, 557–563 (1999)

40. E. Ghiasi, A. Malekzadeh, Removal of various textile dyes using $LaMn(Fe)O_3$ and $LaFeMn_{0.5}O_3$ nanoperovskites; RSM optimization, isotherms and kinetics studies. J. Inorg. Organomet. Polym Mater. **30**, 2789–2804 (2020)

41. M. Bandyopadhyay, S. Dattagupta, Phys. Rev. B **74**, 214410 (2006)

42. P. Singh, M. Shukla, C. Upadhyay, Nanoscale **10**, 22583–22592 (2018)

43. O. Petracic, Superlattices Microstruct. **47**, 569–578 (2010)

44. J.B. Goodenough, A. Wold, R.J. Arnott, N. Menyuk, Relationship between crystal symmetry and magnetic properties of ionic compounds containing Mn3+. Phys. Rev. **124**(2), 373–384 (1961)

45. B. Martinez, V. Laukhin, J. Fontcuberta, L. Pinsard, A. Revcolevschi, Magnetic field and pressure effects on the magnetic transitions of $La_{0.9}Ca_{0.1}MnO3$ perovskites. Phys. Rev. B **66**(5), 54436 (2002)

46. A. Arrott, Criterion for ferromagnetism from observations of magnetic isotherms. Phys. Rev. **108**(6), 1394–1396 (1957)

47. B.-K. Banerjee, On a generalised approach to first and second order magnetic transitions. Phys. Lett. **12**(1), 16–17 (1964)

48. M.H. Phan et al., Complex magnetic phases in LuFe2 O4. Solid State Commun **150**, 341–345 (2010)

49. T.L. Phan, T.D. Thanh, P. Zhang, D.S. Yang, S.C. Yu, The magnetic phase transition and magnetocaloric effect in $Sm_{0.58}Sr_{0.4}2MnO3$ nanoparticles. Solid State Commun. **166**, 32–37 (2013)

50. A. Mleiki, S. Othmani, W. Cheikhrouhou-Koubaa, M. Koubaa, A. Cheikhrouhou, and E. K. Hlil, Effect of praseodymium doping on the structural, magnetic and magnetocaloric properties of Sm0.55-xPrxSr0.45MnO3 (0.1 ≤ x ≤ 0.4) manganites. J. Alloys Compd. https://doi.org/10.1016/j.jallcom.2015.05.043 (2015)

51. D.T. Morelli, A.M. Mance, J.V. Mantese, A.L. Micheli, J. Appl. Phys. **79**, 373 (1996)

52. N. Kallel, S. Kallel. A. Hagaza. M. Oumezzine. Physica. B **404**, 285 (2009)

53. S.K. Barik, C. Krisshnamoorthi, R. Mahendiran, J. Magn. Magn. Mater. **323**, 1015 (2011)

54. D.N.H. Nam, N.V. Dai, L.V. Hong, N.X. Phyc, S.C. Yu, M. Tachibana, E. Takayama, Muromachi, J. Appl. Phys. **103**, 1043905 (2008).

55. A. Belkahla, K. Cherif, J. Dhahri, E.K. Hlil, Large magnetic entropy change and magnetic feld dependence of critical behavior studies in $La_{0.7}Bi_{0.05}Sr_{0.15}Ca_{0.1}Mn_{0.95}In_{0.05}O3$ compound. J. Alloys Compd. **715**, 266–274 (2017)

56. S. Bouzidi, M.A. Gdaiem, S. Rebaoui, J. Dhahri, E.K. Hlil, Large magnetocaloric effect in $La_{0.75}Ca_{0.25-x}Na_xMnO_3$ (0 ≤ x ≤ 0.10) manganites. Appl. Phys. A (2020). https://doi.org/10.1007/s00339-019-3219-z

57. C.A. Taboada-Moreno, F. Sánchez-De Jesús, F. Pedro-García, C.A. Cortés-Escobedo, J.A. Betancourt-Cantera, M. Ramírez-Cardona, A.M. Bolarín-Miró, Large magnetocaloric effect near to room temperature in Sr doped La07Ca03MnO3. J. Magn. Magn. Mater. (2019). https://doi.org/10.1016/j.jmmm.2019.165887

58. S. Kılıç Çetin, G. Akça, A.O. Ayaş, M. Akyol, A. Ekicibil, Structural, magnetic, and magnetocaloric properties of Pb-substituted $La_{0.7}(Te_{1-x}Pb_x)_{0.3}MnO_3$ ($0.0 ≤ x ≤ 0.3$) manganites. J. Supercond. Nov. Magn. **33**, 527–538 (2020)